M. Severin, O. Lammel, W. Meier, Laser diagnostic investigation of a confined premixed turbulent jet flame stabilized by recirculation, Combust. Flame 243 (2022) 112061.

The original publication is available at www.elsevier.com

http://dx.doi.org/10.1016/j.combustflame.2022.112061

Laser diagnostic investigation of a confined premixed turbulent jet flame stabilized by recirculation

Michael Severin[a1], Oliver Lammel[a], Wolfgang Meier[a*]

[a]*German Aerospace Center (DLR), Institute of Combustion Technology, Pfaffenwaldring 38-40, 70569 Stuttgart, Germany*

**Corresponding author: Email address: Wolfgang.meier@dlr.de*

[1] *Present affiliation: Karl Dungs GmbH & Co. KG, Karl-Dungs-Platz 1, 73660 Urbach, Germany*

Key words

Flame stabilization; turbulence-flame interaction; auto-ignition; high-speed PIV and PLIF

Abstract

A preheated premixed CH_4/air jet flame was operated in an optically accessible rectangular combustion chamber in order to study the flame stabilization and flame expansion mechanisms. Due to an off-center position of the jet, a pronounced lateral recirculation zone had formed in the combustion chamber which stabilized the lifted flame by mixing burned and unburned gases in the shear layer. Simultaneous single shot measurements of the flow field by particle image velocimetry (PIV), of OH by planar laser induced fluorescence (PLIF) and of heat release by OH chemiluminescence imaging from two directions were performed at a frame rate of 5 kHz. The image sequences provided a detailed insight into the interaction between the flow field and the flame, particularly into the effects of the vortices that developed in the shear layer between the jet and the recirculation zone. Special interest was devoted to the role of autoignition and turbulent flame propagation near the flame base.

1. Introduction

The stabilization of technically relevant turbulent flames is of significant practical importance and on the other hand also of high relevance for a basic understanding of combustion processes. If we do not consider auxiliary devices such as pilot flames or external ignition sources, there are two major mechanisms left for anchoring and stabilizing flames: Flame propagation and autoignition. In many cases, both mechanisms contribute to flame stabilization, but to different extent and in different locations within a flame. The underlying dynamic processes in turbulent flames and the interaction between autoignition and flame propagation are not yet well enough understood and the development of numerical models requires well-measured test cases with well-defined boundary conditions. In the following, only gaseous turbulent flames that are premixed or partially premixed will be considered, and with a view to applications, gas turbine-like combustion will be predominantly, but not exclusively, considered.

Swirl flames are often used in practical combustors because they offer good flame stability even at high Re numbers. That is because within the vortex-induced recirculating flow, hot combustion products are transported to the flame root where they induce a continuous ignition and flame stabilization by mixing with fresh fuel/air mixtures. Alternative concepts with potentially lower NO_x emissions and less susceptibility to combustion instabilities are based on recirculation induced by

high momentum confined jets. The flameless combustion concept, also termed MILD, FLOX or HiTAC combustion, is one prominent example of this stabilization mechanism [1-5]. This type of combustion is characterized by a homogenization of the flame zone and avoidance of temperature peaks which leads to low NO_x emissions. Of particular importance is the question of the stabilization mechanism of such flames, i.e., the roles of autoignition and flame propagation, as well as the dependencies of stabilization on parameters such as turbulence, temperature, O_2 concentration and some others. It is obvious that autoignition can occur at the conditions prevailing in the mixing zones of hot exhaust gas and fresh gas. Since turbulent flame propagation seemed to also contribute to flame stabilization, the current consensus is that both mechanisms - autoignition and flame propagation - contribute to stabilization. The alternating or simultaneous occurrence of autoignition and flame propagation is, of course, not limited to flameless combustion [6-8] , but the study of this combustion concept has stimulated the discussion of this topic. Therefore, and because the configuration studied in this paper is in principle of flameless-type, some experiments on flameless combustion are shortly addressed in the next paragraph.

In order to understand the details of flameless combustion and the stabilization mechanism, numerous investigations have been carried out under simplified conditions. In order to classify the configuration studied in this paper (a premixed jet enclosed by a non-axisymmetric burn chamber) within the framework of arrangements known from the literature, they are briefly summarized here. For details please refer to the mentioned review articles and the citations therein. Jet-in-hot-coflow (JHC) configurations have been extensively studied experimentally and numerically. Such arrangements mimic the intense mixing of recirculated flue gas with fresh gas taking place in practical systems by a co-flow of vitiated air surrounding a central jet of fuel or fuel-air mixture. Most of these studies have been performed for non-premixed fuel jets and only a few for premixed fuel-air jets [9-11]. The co-flow temperatures were typically in a range between 1000 and 1600 K and the O_2 concentration were around 10%. Unconfined configurations enabled relatively easily the application of laser diagnostics to determine the flow velocities, temperature and species concentrations. Confined flames were studied to a lesser extent in various arrangements. Kruse et al. [12] and Ye et al. [13] used a reverse flow combustor at atmospheric and elevated pressure and determined the emissions but without applying laser diagnostics. The group of Mário Costa studied a confined configuration with a central air nozzle surrounded by a ring of fuel nozzles [14] by applying probe techniques for temperature and species. More complex configurations were studied by Sidey [15] and in the groups of Ashwani Gupta [16] and Antonio Cavaliere [17]. The review article of Perpignan et al. [3] yields a good compilation and overview of the studies.

While the maximum temperature in MILD combustion is much lower than 1600 °C [5] modern heavy duty gas turbines are designed for turbine inlet temperatures above 1600 °C and it is this temperature range of interest for the investigations presented here. A clear difference of the flame examined here to flameless combustion is furthermore the presence of flame fronts. The background for the research presented in this article originated from the development of burners with jet-stabilized flames for large gas turbines. A typical nozzle arrangement of such a burner is displayed in Fig.1. Each of the 12 nozzles that are arranged on a ring injects partially premixed natural gas and air with high velocity into the combustion chamber. The flame length is on the order of 10D where D is the exit diameter of the nozzles and the flow field is characterized by a large central recirculation zone which plays the dominant role for the flame stabilization. Historically, the burner is termed FLOX® combustor, although the combustion is in most cases not flameless. However, it exhibits

essential features of flameless combustion such as dilution of fresh charge with exhaust gas, extended flame zone and reduced NOx emissions. The burner has been operated in a high-pressure test-rig in various configurations [15-17] and recently in a configuration with a single large nozzle that was placed out of axis in a square combustion chamber, see Fig.2 [18-22]. The single-nozzle burner mimics to a certain extent one section of the circularly arranged FLOX® combustor. It was operated with air preheated to 673-823 K, pressures up to 8 bar and equivalence ratios in the range of 0.7-0.28. At these conditions, the combustion temperature was rather high, typically around 1900 K. A high combustion and turbine inlet temperature is desired to achieve a high turbine efficiency. The combustion was not flameless, however, there were clear indications of autoignition in the mixing zone of recirculated and fresh gas. In a numerical study of this flame, Gruhlke et al. concluded that the flame is stabilized by propagation assisted by autoignition [18].

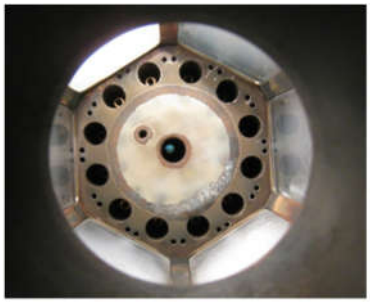

Fig. 1: Photo of a confined FLOX burner with 12 nozzles for the injection of fuel-air mixtures.

Fig. 2: Photo of a confined single-nozzle jet burner of industrial scale installed in a high-pressure test-rig. The 7 small nozzles can be used to optionally operate a pilot flame.

In order to better understand the dynamic processes and the stabilization mechanism within this configuration a laboratory-scale experiment was set up for flames operated with perfectly premixed CH_4 and preheated air at atmospheric pressure, confined in a rectangular combustion chamber with optical access. To investigate physical and chemical combustion processes non-intrusively, optical and laser-based measurement techniques have established themselves as the method of choice [19-25] and were therefore used in this experiment. Because autoignition and turbulent flame propagation are dynamic and three-dimensional processes, high-speed imaging techniques were applied to measure the flow velocities by Particle Image Velocimetry (PIV), to visualize the OH

distribution by planar laser-induced fluorescence (PLIF) and to image OH chemiluminescence (OH* CL) from two directions. The techniques were applied simultaneously at a repetition rate of 5 kHz. This complex detection setup enabled the identification of isolated ignition kernels and, in case the ignition kernels were within the laser sheets, the temporal development of the kernels and the boundary conditions with respect to OH and velocity distributions. It also enabled the tracking of reaction zones and their interactions with the flow field. Overall, the measurements provided a comprehensive picture of the stabilization mechanism in this flame configuration and the results are well-suited for the improvement and validation of numerical models.

Literature about configurations comparable to the current one is scarce. To the authors' knowledge, a confined turbulent recirculation stabilized jet flame has not been studied before elsewhere, at least not with temporally resolved laser techniques. The high-pressure single-nozzle FLOX® combustor shown in Fig.2 is very similar in terms of configuration, but was not studied by high-speed imaging techniques. A configuration that is somehow related with the one presented here, is the jet-in-crossflow (JICF) arrangement. Several experimental and numerical studies have been performed for premixed jets in hot vitiated crossflows, see for example [26-30]. A general finding was that autoignition assisted the flame stabilization, particularly on the windward side, and that also turbulent flame propagation contributed to flame stabilization. However, the burner geometry and the flow field in a JICF configuration are quite different from the one studied in this paper.

2. Experimental

2.1 Model combustor and operating conditions

Figure 3 shows a schematic drawing of the model combustor. The vertically arranged combustion chamber has a cross section of 50 mm × 40 mm, a length of 600 mm and is open at the top. All four

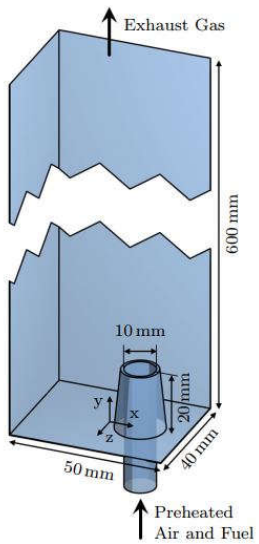

Fig. 3: Schematic drawing of the model combustor with definition of the co-ordinate system.

sides consist of quartz glass plates of 8 mm thickness and 200 mm length, held by a water-cooled metal frame. In axial direction the combustion chamber is composed of three segments, each 200

mm high which are arranged one above the other. The burner base plate is made of a ceramic material to reduce heat loss to the water-cooled base plate below. The jet nozzle is a stainless steel pipe with an inner diameter of 10 mm, tapered at the exit. For better optical access to the start region of the jet the nozzle protrudes by 20 mm into the combustion chamber. The origin for the coordinate system used in this paper is placed at the center of the burner base plate. x denotes the horizontal direction, y the vertical direction, and z the lateral direction in which the setup is symmetric. The flames were operated with premixed CH_4 and air preheated to a temperature of 473 K by an electrical heater (see Fig.4). The temperature was monitored by a thermocouple approximately 100 mm upstream of the nozzle exit. The air and CH_4 mass flows were controlled by mass flow controllers (Brooks). In previous experiments the flame behavior was studied in a wide range of jet exit velocities (1-300 m/s) and air excess ratios (λ = 1.0-1.6) [31][Severin 2017]. The current experiments with detailed laser diagnostics were performed for mass flows of 62.8 g/min (air) and 3.64 g/min (CH_4), yielding an equivalence ratio of ϕ = 1, a mean jet exit velocity of 20 m/s and a nozzle exit Re number of 5640.

2.2 Experimental arrangement and measurement techniques

The measurement setup with the lasers and detectors is displayed in Fig. 4. Unless otherwise stated, the measurement techniques were applied at 5 kHz repetition rate. For the application of stereoscopic Particle Image Velocimetry (PIV) the flow was seeded with TiO_2 particles with a diameter of 1 µm. A high speed twin head diode-pumped Nd:YAG laser (EdgeWave InnoSlab IS200-2-LD) with a wavelength of λ=532 nm was used for the illumination of the seeded flow. The laser beam was formed into a sheet with a set of cylindrical lenses, resulting in a sheet of 115 mm height with a thickness of 1.0 mm in the measurement volume. The laser sheet was adjusted to match the symmetry plane of the combustor at z = 0 mm. The double pulse separation time was 40 µs. Two high speed cameras (LaVision HighSpeedStar 8), equipped with an optical bandpass filter (532 ± 5 nm), were used in double frame mode to record the PIV images. The cameras were inclined at an angle of 30° in order to perform stereoscopic PIV, resulting in the determination of all three velocity components. The PIV images were processed with a commercial software (LaVision DaVis 8.3) on a single shot basis and statistically analyzed in MatLab.

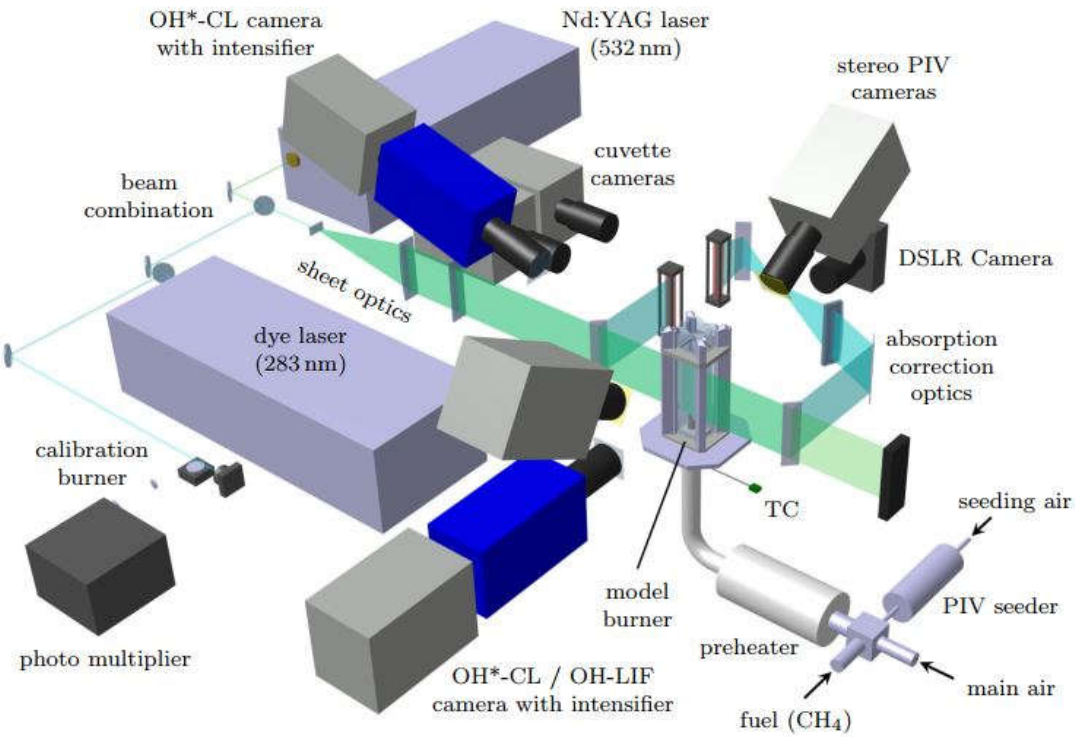

Fig. 4: Arrangement of the measurement setup. The combustion chamber is shown in a broken view for the sake of clarity. TC stands for thermo couple, DSLR for digital single lens reflex camera.

Two-dimensional laser induced fluorescence (LIF) of the OH radical was measured to obtain a qualitative information on the fluid's thermochemical state, e.g. to distinguish between unburned and burned gas. For the OH LIF measurements, a high speed dye laser (Sirah Credo Dye) tuned to λ= 283.305 nm was used to excite the $Q_1(7)$ transition within the 0 → 1 vibrational band of the OH *A - X* band system. The LIF laser beam was combined with the PIV laser beam ahead of the sheet forming optics, so that a sheet in the same direction with a similar height is formed. This simplifies the experimental setup, but has the disadvantage that the laser sheets cannot be adjusted independently, so that the sheet optimization with respect to parallelism and focus was a compromise between the two wavelengths. The thickness of the LIF laser sheet in the combustion chamber was approximately 0.4 mm. The OH LIF signal was captured by a high speed CMOS camera with a high speed image intensifier (Phantom V1212 and LaVision HS-IRO), equipped with a UV lens (f=100 mm, B. Halle Nachf.) and a bandpass filter (λ=310±20 nm). The exposure time was set to 100 ns and temporally between the PIV laser pulses. A small portion of the LIF laser sheet ahead and after the measurement volume was reflected into a reference cuvette filled with dye solution and the luminescence of each cuvette was imaged by another high speed camera (2× LaVision HighSpeedStar 5), to determine the intensity distribution of the laser sheet. The intensity distribution in the first cuvette was used to normalize the LIF signal to the incoming laser energy (in the vertical direction). The intensity distribution in the second cuvette was used to normalize the LIF signal to the laser attenuation caused by the OH absorption in beam direction. To distinguish between the laser attenuation by OH absorption and by other factors such as stained combustion chamber windows, a reference measurement was performed with the LIF laser tuned to a wavelength slightly off the OH resonance line. The processing and statistical analysis of the LIF images was done with an in-house

MatLab code. A small portion of the laser beam was coupled out and directed into a premixed CH_4/air flame stabilized on a small matrix burner (calibration burner). The laser induced fluorescence from this reference flame was detected by a photomultiplier tube and used to ensure that the laser wavelength was exactly on the OH resonance.

The camera used for OH PLIF detection was also used to image OH chemiluminescence (OH* CL) in the y-x-plane, however, with a longer gate time of 20 µs which ended 15 µs before the PLIF laser pulse. A second high speed camera with intensifier, optical filter system and Scheimpflug adapter was arranged perpendicularly to the first one to imaging the OH* CL in the y-z-plane. This camera had to be placed at a slightly inclined angle of 12° above the laser sheet to avoid blocking of the laser sheet. OH* CL from flames is a good qualitative marker of global heat release [32-34] and can be used to identify flame kernels. To obtain coarse spatial resolution from the line-of-sight integrated OH* CL images and to identify the position of auto-ignition kernels relative to the laser sheets, OH* CL was acquired from two spatial directions [35] . Finally, a digital single-lens reflex (DSLR) camera was used to take photos of the flame (Canon EOS 500D) for documentation, in this case not at high repetition rate.

20,000 images (or double images) were recorded for each PIV, OH PLIF and OH* CL in one measurement series corresponding to a total measurement time of 4 s. The resulting simultaneously acquired time series enabled the identification of effects such as autoignition, flame jumps, flame roll-up or local flame extinction.

3. Results and discussion

3.1 General flame appearance

Figure 5 shows a photo of the flame and the combustion chamber. Obviously, the flame is lifted and asymmetric with respect to the nozzle axis. The flame fluctuates somewhat but burns stably. The visible flame length lies within the lowest segment. Mean values of the OH* CL, the flow velocities and the OH LIF are displayed in Fig.6. These distributions were averaged over 20,000 shots within one measurement series. The OH* CL distribution (a) resembles the visible flame appearance in the photo, as expected. It is seen that the lift-off height is approximately 60 mm from the nozzle exit ($y \approx 80$ mm) and the intensity maximum is at $y \approx 140$ mm.

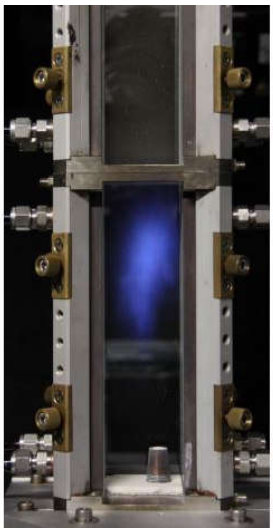

Fig. 5: Photo of the flame and the combustion chamber.

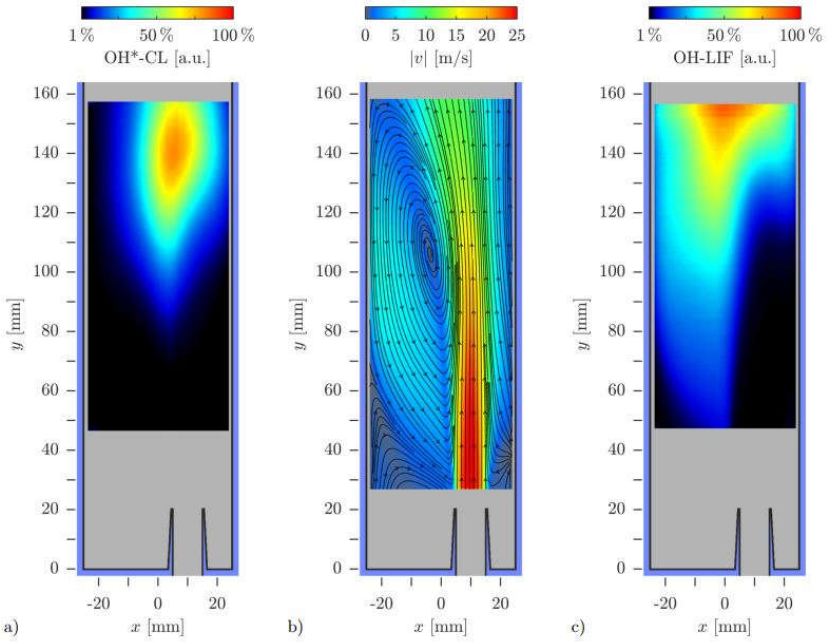

Fig. 6: Ensemble-averaged distributions of the line-of-sight integrated OH chemiluminescence (OH* CL), flow velocities and OH LIF in the x-y-plane. The velocity distribution is composed of two averaged distributions measured with a displacement of Δy = 20 mm in order to capture also the flow field near the nozzle.

The corresponding averaged flow field (b) results from two measurement series, where the laser sheet was displaced by -20 mm in y direction for the second series in order to also capture the velocity distribution in the vicinity of the nozzle exit. The arrows indicate the flow direction and the colors represent the magnitude of the axial velocity. The mean flow field in this section plane can be divided into three zones: The high momentum jet that exceeds to y > 160 mm, the large, clearly pronounced lateral recirculation zone on the left side and a smaller recirculation region near the nozzle which is only partly mapped because this region was not completely accessible to the laser

sheet. The reverse flow in the lateral recirculation zone transports hot exhaust gas to the start region of the jet where it mixes with unburned gas. As in other flames with recirculation this flow feature builds the dominant mechanism for the stabilization of the flame. However, the details of this mechanism cannot be deduced from the averaged distributions and will be discussed on the basis of correlated single shot images. It is noted that the mean flow field in z direction is mirror symmetrical with respect to the nozzle axis. From PIV measurements in a similar burner setup it is known that the lateral recirculation flow encompasses the jet root outside the measurement plane, so that hot exhaust gas also reaches the opposite side of the jet. In addition, the reverse flow and the burner geometry lead to corner recirculation zones in the lower part of the combustion chamber. However, they do not play an important role for the flame stabilization.

Figure 6 (c) shows the average OH distribution. OH (in the electronic ground state) can be found in detectable concentrations at temperatures above approximately 1400-1500 K in lean flames and the equilibrium concentration increases exponentially with temperature. It is formed in superequilibrium concentrations in the reaction zones and its relaxation to equilibrium by three-body collisions is quite slow at atmospheric pressure ($\tau \approx 3$ ms) [36] . The gradients within single-shot OH distribution are therefore sometimes used to identify reaction zones. The maximum mean OH signal occurs close to the region of the maximum heat release, as expected, because of superequilibrium OH and high temperatures in the flame and post-flame region. From UV laser absorption measurements in this flame it is known that the maximum of the color scale corresponds roughly to temperatures of 2200 K, while the minimum of the color scale corresponds to temperatures around 1500 K. The relatively high temperatures in the lateral recirculation zone confirm that hot exhaust gas is recirculated here. The change of the OH distribution with height at the left combustor wall also indicates heat loss of the flow during the recirculation.

3.2 Time resolved correlated single shot measurements

While the averaged distributions give a general impression of the flame, correlated single shot images must be analyzed to reveal details of the turbulence-flame interaction and flame stabilization. Figure 7 displays an example of simultaneously recorded distributions of (line-of-sight integrated) OH* CL from two directions as well as velocity fields and OH LIF in the x-y-plane. For convenience, OH* CL distributions recorded with short exposure time (20 µs) are also called single shot distributions, although no laser is involved. In the OH* CL distributions a white contour line marks the boundary of the signal to facilitate the distinction between reacting and non-reacting regions. Its distribution in the x-y-plane shows a contiguous area that resembles the mean distribution in Fig. 6. In contrast, the distribution in the z-y-plane exhibits isolated reacting fluid elements in the stabilization region of the flame. These may either reflect autoignition events or flame fragments that have been stripped off of a contiguous flame by the turbulent flow field or they are remains of local flame extinction. Such isolated areas were also observed further downstream in the edge region of the flame. From just one single-shot image it is difficult to decide the origin of such events.

The instantaneous flow field displayed in the third image of Fig.7 shows a series of vortices in the shear layer between the jet and the lateral recirculation zone that combine to a contiguous recirculating flow farther away from the jet. As in the mean values of Fig.6 relatively high velocities of the jet core are seen up to the upper edge of the image. Shear layer-generated vortices are only

present on the left side where the distance between the shear layer and the left wall is approximately 30 mm. On the right side where the distance between the shear layer and the right wall is only approximately 10 mm such vortices were almost never observed. The corresponding OH LIF distribution, presented in the fourth image, shows high (presumably superequilibrium) OH concentrations and large spatial gradients above y ≈120 mm. They are indications of reacting areas and flame fronts. This interpretation is supported by the OH* CL images which show reacting regions above y ≈120 mm from both observation directions. The dashed line in the OH* CL image in the z-y-plane that indicates the position of the OH PLIF laser sheet clearly proves that the laser sheets intersects reacting regions. The comparison between the OH* CL and OH PLIF distributions also suggests that the regions in the OH PLIF field with elevated signal levels (yellow) at y ≈90 mm and between y ≈ 100 mm and 110 mm represent flame fronts. The comparatively small OH LIF signals below y ≈ 85 mm reflect reacted gas with temperature slightly above approximately 1500 K. The corresponding OH* CL distributions confirm that there is no flame in this region. The changes of the OH LIF intensities near the left wall indicate some heat loss of the recirculating flow on its way down.

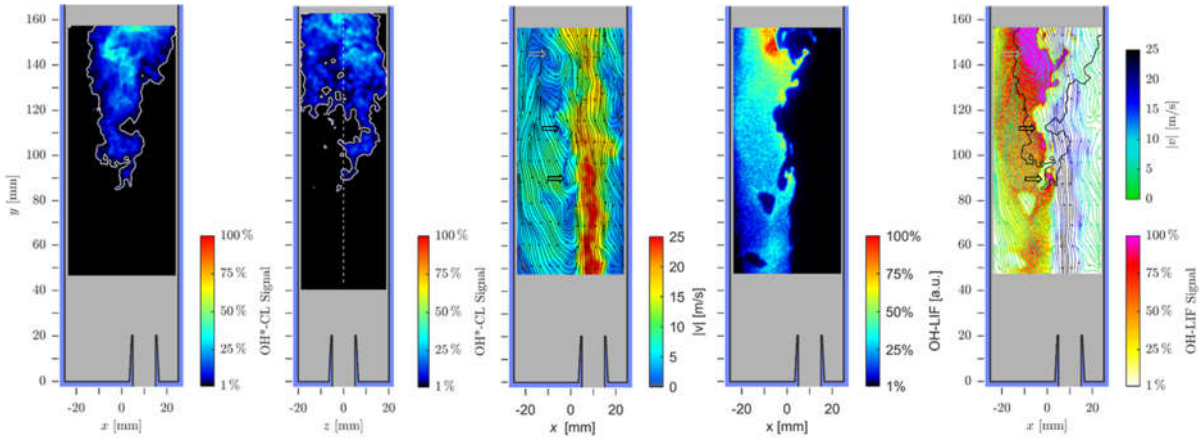

Fig. 7: Example of simultaneously measured single shot distributions. 1. OH* CL in the x-y-plane; 2. OH* CL in the z-y-plane. The dashed line indicates the position of the PIV and OH PLIF laser sheets; 3. Velocity distribution; 4. OH PLIF distribution; 5. OH LIF signal overlaid by color coded instantaneous streamlines from PIV in the x-y-plane, and the contour of the OH* CL in the same plane.

As an attempt to include the information from these images into one frame, OH LIF, the flow velocities and the OH* CL in the x-y-plane are overlaid in the fifth image in Fig.7. Note that the color bars have been changed to distinguish between the different quantities. The OH* CL contour in the x-y-plane is shown as a black line. Several observations can be made. The flame sheets at y ≈ 90 mm and between y ≈ 100 mm and 110 mm seen in the OH PLIF distributions reside in the shear layer between the jet and the lateral recirculation zone. On the left side of these flame sheets there are two vortices with their centers at y ≈ 90 mm and y ≈ 110 mm, indicated by black arrows in Fig.7. They mix hot recirculated gas into the jet and fresh gas from the jet into the recirculation zone. It is apparent that the mixing of exhaust gas and unburned fresh gas at the positions mentioned initiate the ignition and/or favor the expansion of the flame. Further downstream, around x ≈-6 mm and y ≈ 148 mm, the OH distribution shows a relatively large reacting region. A little left of this region lies the center of another vortex (see gray arrow in Fig.7) which enhances the mixing of fluids from the jet and the recirculation zone. From this example single shot composition, and also from the mean values in Fig.6, it can be concluded that above y ≈ 120 mm combustion is far advanced, there is a

contiguous flame and there is no hint that autoignition is of significant role. Below y ≈ 120 mm the situation is more complex and must be analyzed further.

In the following, excerpts from the time series are considered. Figure 8 shows a time sequence of 4 single shots in the style of the overlaid distributions of Fig. 7 together with the corresponding OH* CL images in the z-y-plane. To save space, the sequence is not shown here with full temporal resolution of 0.2 ms, instead the time intervals have been chosen so that the flame changes can be well recognized. The characteristic vortices in the shear layer between the jet and the lateral recirculation zone are clearly seen. They generate a mixing of fresh gas from the jet and recirculated exhaust gas and in this way they contribute significantly to the characteristics of the flame and its stabilization.

An example of this process is seen at y ≈ 105 mm (see arrows in Fig. 8). At the time t = 278.8 ms, this vortex mixes fresh gas and exhaust gas by pushing hot exhaust gas into the jet below the vortex center and transporting unburned fresh gas into the recirculation zone above the vortex center. According to the OH* CL distribution in the z-y-view, a reacting flame is present below the vortex center, while a non-reacting interface is present to the left and above the vortex. In the next time step at t = 279.4 ms the reacting flame front has been transported downstream by the vortex along its right side (possibly also with a contribution of flame propagation) and shows maximum OH LIF intensity. The further temporal development of the LIF distribution shows that this flame expands into a region with small OH concentrations (yellow OH LIF intensity), i.e. into a region with mixtures of burned and unburned gases. At the same time, the flame and the burned gas are convected downstream while a portion of them finds its way into the recirculation zone. Finally, at y ≈ 150 mm only burned gas is present, at least in the plane of the laser light sheet. This process of vortex-induced mixing, flame wrap-up and flame expansion can be seen in almost all image sequences and triggers the predominant part of the flame reactions. It cannot be completely ruled out that autoignition also contributes to the flame expansion described, but the structures visible in the OH distributions and in the OH gradients indicate propagating flame fronts. Apart from a few autoignition events seen in Fig. 8, the main body of the flame is stabilized at y ≈ 100 mm and the distribution of the mean OH* CL values in Fig.6 prove that this happens predominantly on the side with the lateral recirculation zone. The instantaneous OH* CL distributions in Fig.8 show a contiguous flame body in this region which suggests that the flame propagates here, near the shear layer, against the direction of flow. A determination of the local flame speed from these measurements is, however, not possible because of the three-dimensional nature of the flame topography which cannot be captured by the line-of-sight integrated OH* CL images and a single-plane OH PLIF distribution [37, 38].

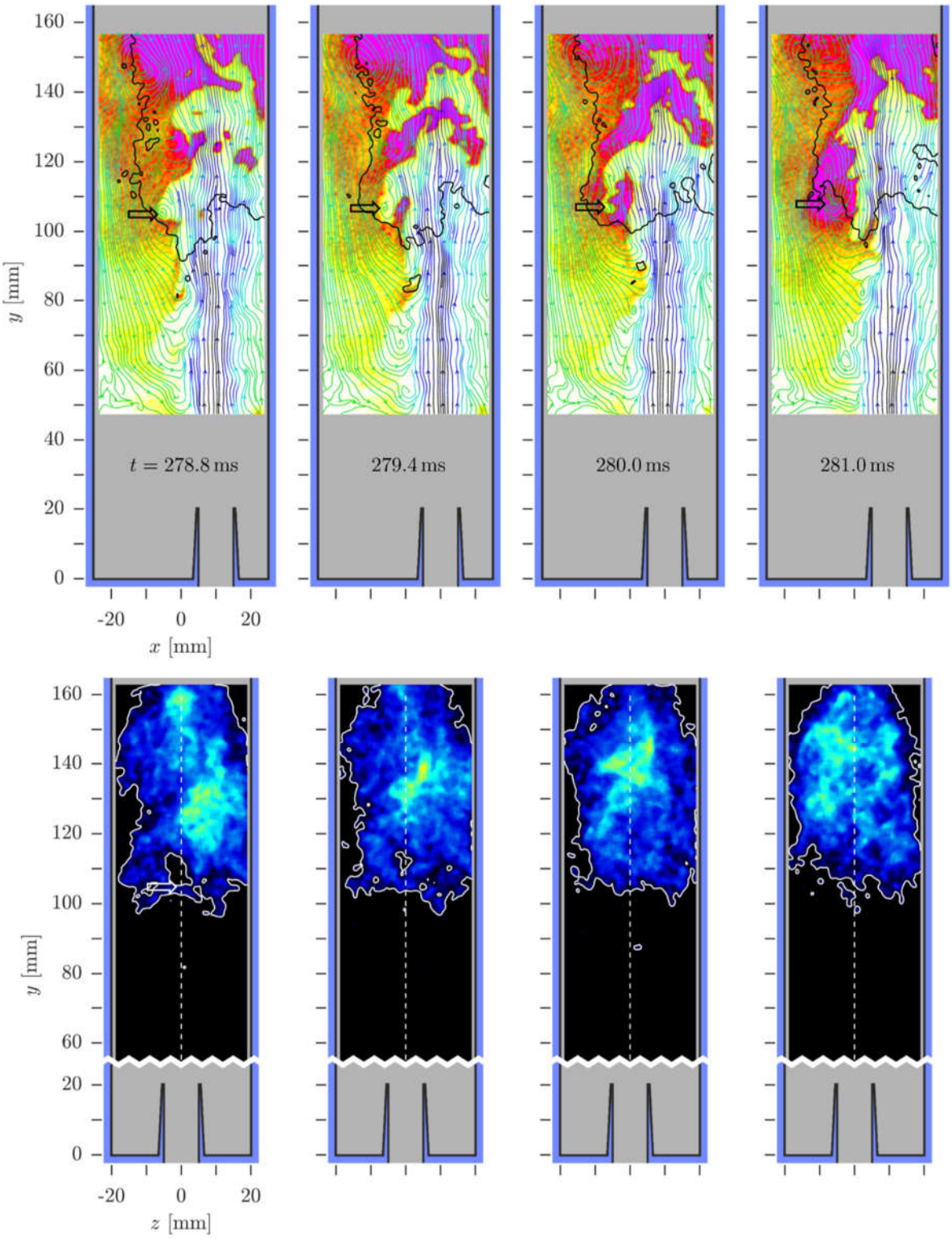

Fig. 8: Example of a time sequence of overlaid single-shot distributions and corresponding (line-of-sight integrated) OH* CL images in the z-y-view. The displayed time steps have been chosen to illustrate the effects of the vortices in the shear layer on the flame development.

Another example of a time sequence is displayed in Fig.9. A larger number of autoignition events is seen in this case, and the stabilization region is more structured than in the previous example. The typical action of the vortices in the shear layer is also seen here, e.g. at y ≈ 105 mm. However, in this case the isolated flame kernels near y = 100 mm are clearly due to autoignition. Subsequently, the

kernels grow and merge and finally combine with the main flame body at t ≈ 695,6 ms while at other locations new flame kernels appear, e.g. at y ≈ 110 mm, x ≈ -12 mm. Thus, this sequence demonstrates that autoignition can play an important role for the stabilization of this flame. The flame would certainly burn even without the appearance of the autoigniting flame kernels, but the location of the flame anchoring region can be significantly influenced by autoignition. This also becomes clear when analyzing the temporal development of the lift-off height as displayed in Fig.10. Here the lift-off height was determined as the lowest y position where the OH* CL intensity exceeded a threshold value in each single shot of a time sequence recorded at 5 kHz. In the displayed time interval of 40 ms, the lift-off height varies between y = 56 mm and 97 mm and exhibits a sawtooth profile. The sudden decreases of the lift-off height (marked in red) are explained by the appearance of autoignition kernels below the main flame body [39]. The slow increase in lift-off height is typical of the growth and convection of the flame kernels. Sudden increases of the lift-off height (marked in green) are explained by local extinction of flame kernels or disrupted flame fronts. The analysis of the whole measurement series with a total duration of 1s results in 258 autoignition events and 175 local extinction events. A discontinuity height of at least 5 mm in positive or negative direction (within the resolved time step of 0,1 ms) was used as the criterion to identify, count and mark these events automatically. The criterion of 5 mm is rather conservative and was chosen to match the visual impression from the corresponding OH* CL and OH PLIF series, that could clearly be identified as autoignition events. Smaller autoignition events in the close vicinity of the flame root or rapid consecutive autoignition events cannot clearly be distinguished from flame propagation via turbulent vortices with the used experimental setup. The detected number of autoignition events corresponds to an average occurrence frequency of roughly once every 4 ms and can be seen as a lower limit for the actual number of autoignition events.

Further examples of time sequences like those shown in Fig. 8 and 9 are given in the Ph.D. dissertation of M. Severin [40]. They support the conclusion that autoignition definitely takes place at the flame root, that it is difficult to specify the influences of autoignition and flame propagation in the flame anchoring region (the zone where the main body of the flame starts) and that the predominant part of combustion seems to be taking place by flame propagation.

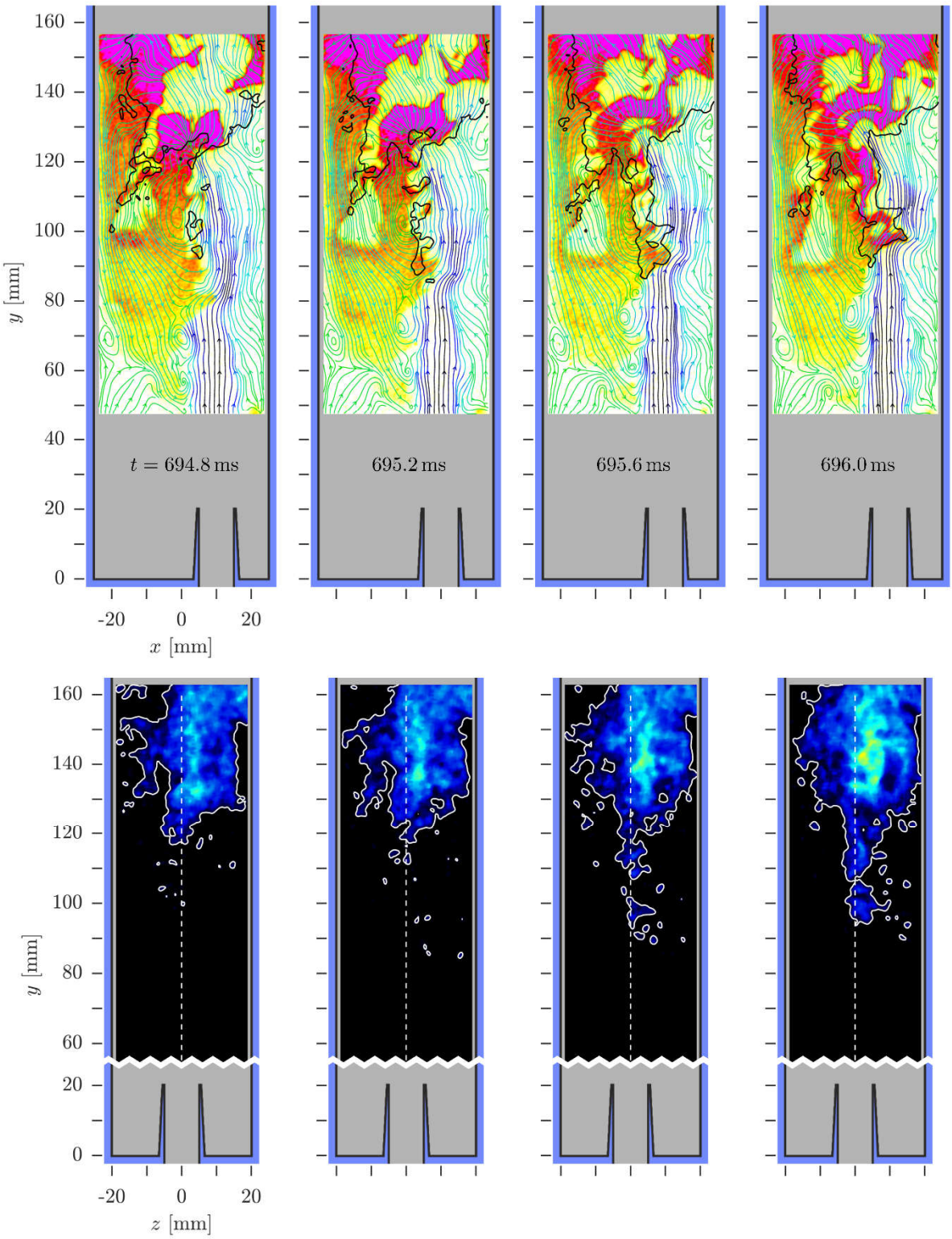

Fig. 9: A second example of a time sequence of overlaid single-shot distributions and corresponding (line-of-sight integrated) OH* CL images in the z-y-view. The displayed time steps have been chosen to illustrate the development of the autoignited flame kernels.

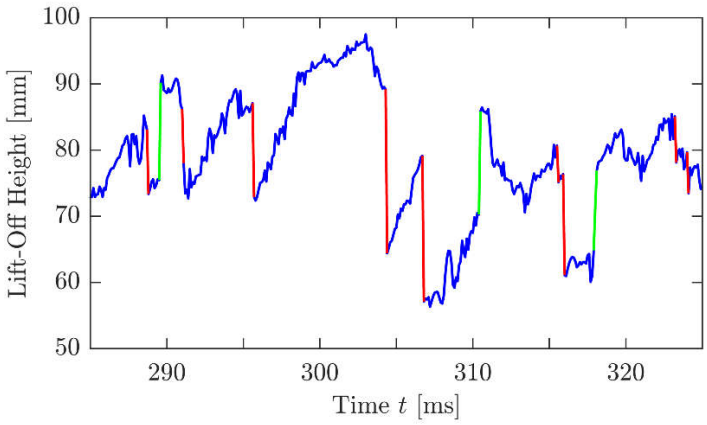

Fig. 10: Development of the flame lift-off height with time, deduced from highspeed OH* CL time series. Red and green parts of the graph mark sudden decreases and increases, interpreted as autoignition events and extinction events, respectively.

4. Summary and conclusions

A single-nozzle burner for confined premixed CH_4-air jet flames has been set-up as a simplified laboratory-scale configuration of a gas turbine burner for jet-stabilized flames. The aim of this work was to study the flame stabilization mechanism and in particular the contribution of autoignition and flame propagation to it. Although the configuration is also suitable for flameless combustion, the operating conditions (ϕ = 1, $T_{preheat}$ = 473 K) were chosen to stabilize a visible flame with relatively high combustion temperatures which are similar to those in large gas turbines. The flame was lifted and exhibited a pronounced lateral recirculation zone.

An optically accessible combustion chamber enabled the application of PIV for the measurement of the flow field, OH LIF for the visualization of OH distributions and OH chemiluminescence imaging from two sides for the identification of flame zones. These techniques were applied simultaneously at a frame rate of 5 kHz and delivered time series of 20,000 frames. The time series were used to analyze the temporal development of the flow field-flame interaction and the appearance or extinction of flame kernels.

Processes essential for the flame behavior took place in the shear layer between the jet and the lateral recirculation zone. The cartoon in Fig. 11 illustrates these processes schematically. In the shear layer, a number of vortices with a typical size of 5-8 mm induce a mixing of fresh gas from the jet and recirculated burned gas. The mixture ignites, the reacting gas is wrapped up by the vortex while the combustion progresses, the flame expands and finally merges with the main body of the flame. A similar flame wrap-up and expansion occurs when a vortex pushes a part of a flame front into the jet. This sequence of processes triggers the predominant part of the flame reactions. It cannot be completely excluded that autoignition also contributes to the flame expansion described, but the structures in the OH distributions and their gradients indicate propagating flame fronts.

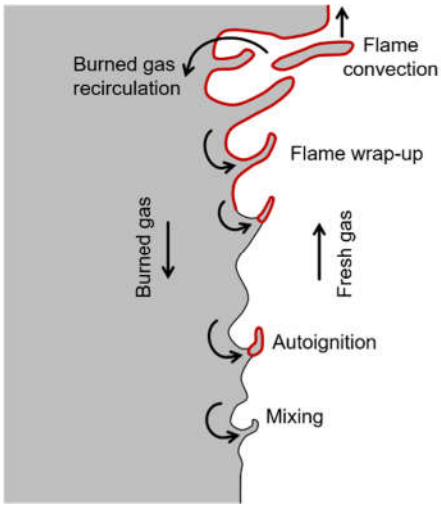

Fig. 11: Schematic illustration of the processes in the shear layer between the jet and the lateral recirculation zone.

However, autoignition events frequently occur below the main flame body and are clearly identified by the OH* CL distributions. 258 autoignition events within one second have been identified in the presented measurement. They are mostly initiated by the mixing induced by the vortices in the shear layer. Typically, isolated flame kernels grow, may merge with other flame kernels and finally combine with the main flame body. Such autoignition events have a significant influence on the lift-off height of the flame, as demonstrated by the sawtooth shape of the time sequence of the lift-off height. However, there were no clear indications that autoignition contributes to the flame expansion and reaction progress in the main body of the flame further downstream.

The influence of autoignition on flame propagation is difficult to assess from the present measurement data. It is clear that the mixing of hot exhaust gas and fresh gas leads to the formation of flame precursors below the main flame body. Mixtures formed in this way support flame propagation and enable autoignition further downstream. If autoignition occurs in the immediate vicinity of flame fronts it becomes difficult to distinguish flame expansion by autoignition from flame propagation. Simultaneous high-speed PLIF measurements of CH_2O and OH in combination with OH* CL imaging could possibly provide more clarity. However, even then caution must be taken using CH_2O as marker for autoignition in flames with mixed stabilization modes [41].

Even if the interaction between the flame and the flow field in the configuration presented here is partly purely phenomenological, the time sequences of simultaneous measurement data show the processes in the flame in a detail that is hardly feasible in high-pressure experiments on a similar configuration. For a deeper understanding of the physical and chemical processes discussed here, numerical simulations would be helpful, for which the experimental results of this work can serve as a validation case. The authors would appreciate a numerical experiment using Large Eddy Simulation with detailed chemistry, where the influence of flame propagation and autoignition can be monitored (e.g. via ignition precursors) or systematically manipulated by parameter variation.

Acknowledgement

Wolfgang Meier would like to thank Katharina Kohse-Höinghaus for numerous fruitful discussions and for many years of scientific exchange and friendship.

References

[1] J.A. Wünning, J.G. Wünning, Flameless oxidation to reduce thermal no-formation, Progress in Energy and Combustion Science 23 (1997) 81-94.
[2] A. Cavaliere, M. de Joannon, MILD combustion, Progress in Energy and Combustion Science 30 (2004) 329-366.
[3] A.A.V. Perpignan, A. Gangoli Rao, D.J.E.M. Roekaerts, Flameless combustion and its potential towards gas turbines, Progress in Energy and Combustion Science 69 (2018) 28-62.
[4] R. Weber, A.K. Gupta, S. Mochida, High temperature air combustion (HiTAC): How it all started for applications in industrial furnaces and future prospects, Applied Energy 278 (2020) 115551.
[5] J. Mi, P. Li, F. Wang, K.-P. Cheong, G. Wang, Review on MILD Combustion of Gaseous Fuel: Its Definition, Ignition, Evolution, and Emissions, Energy & Fuels 35 (2021) 7572-7607.
[6] O. Schulz, T. Jaravel, T. Poinsot, B. Cuenot, N. Noiray, A criterion to distinguish autoignition and propagation applied to a lifted methane–air jet flame, Proceedings of the Combustion Institute 36 (2017) 1637-1644.
[7] J.F. Driscoll, J.H. Chen, A.W. Skiba, C.D. Carter, E.R. Hawkes, H. Wang, Premixed flames subjected to extreme turbulence: Some questions and recent answers, Progress in Energy and Combustion Science 76 (2020) 100802.
[8] A.M. Steinberg, P.E. Hamlington, X. Zhao, Structure and dynamics of highly turbulent premixed combustion, Progress in Energy and Combustion Science 85 (2021) 100900.
[9] M.J. Dunn, A.R. Masri, R.W. Bilger, A new piloted premixed jet burner to study strong finite-rate chemistry effects, Combustion and Flame 151 (2007) 46-60.
[10] C. Duwig, B. Li, Z.S. Li, M. Aldén, High resolution imaging of flameless and distributed turbulent combustion, Combustion and Flame 159 (2012) 306-316.
[11] J. Si, G. Wang, J. Mi, Characterization of MILD Combustion of a Premixed CH4/Air Jet Flame versus Its Conventional Counterpart, ACS Omega 4 (2019) 22373-22384.
[12] S. Kruse, B. Kerschgens, L. Berger, E. Varea, H. Pitsch, Experimental and numerical study of MILD combustion for gas turbine applications, Applied Energy 148 (2015) 456-465.
[13] J. Ye, P.R. Medwell, E. Varea, S. Kruse, B.B. Dally, H.G. Pitsch, An experimental study on MILD combustion of prevaporised liquid fuels, Applied Energy 151 (2015) 93-101.
[14] A.S. Veríssimo, A.M.A. Rocha, M. Costa, Importance of the inlet air velocity on the establishment of flameless combustion in a laboratory combustor, Experimental Thermal and Fluid Science 44 (2013) 75-81.
[15] J. Sidey, E. Mastorakos, Visualization of MILD combustion from jets in cross-flow, Proc. Combust. Inst. 35 (2015) 3537-3545.
[16] A.E.E. Khalil, A.K. Gupta, On the flame–flow interaction under distributed combustion conditions, Fuel 182 (2016) 17-26.
[17] G. Sorrentino, P. Sabia, M. de Joannon, A. Cavaliere, R. Ragucci, The Effect of Diluent on the Sustainability of MILD Combustion in a Cyclonic Burner, Flow, Turbulence and Combustion 96 (2016) 449-468.
[18] P. Gruhlke, H. Janbazi, I. Wlokas, C. Beck, A.M. Kempf, Investigation of a High Karlovitz, High Pressure Premixed Jet Flame with Heat Losses by LES, Combustion Science and Technology 192 (2020) 2138-2170.
[19] K. Kohse-Höinghaus, R.S. Barlow, M. Aldén, J. Wolfrum, Combustion at the focus: laser diagnostics and control, Proceedings of the Combustion Institute 30 (2005) 89-123.

[20] B. Böhm, C. Heeger, R.L. Gordon, A. Dreizler, New Perspectives on Turbulent Combustion: Multi-Parameter High-Speed Planar Laser Diagnostics, Flow Turbulence and Combustion 86 (2011) 313-341.
[21] M. Aldén, J. Bood, Z. Li, M. Richter, Visualization and understanding of combustion processes using spatially and temporally resolved laser diagnostic techniques, Proc. Combust. Inst. 33 (2011) 69-97.
[22] V. Sick, High speed imaging in fundamental and applied combustion research, Proceedings of the Combustion Institute 34 (2013) 3509-3530.
[23] A. Ehn, J. Zhu, X. Li, J. Kiefer, Advanced Laser-Based Techniques for Gas-Phase Diagnostics in Combustion and Aerospace Engineering, 71 (2017) 341-366.
[24] K. Kohse-Höinghaus, Clean combustion: Chemistry and diagnostics for a systems approach in transportation and energy conversion, Progress in Energy and Combustion Science 65 (2018) 1-5.
[25] M.J. Evans, P.R. Medwell, Understanding and Interpreting Laser Diagnostics in Flames: A Review of Experimental Measurement Techniques, 5 (2019).
[26] D. Schmitt, M. Kolb, J. Weinzierl, C. Hirsch, T. Sattelmayer, Ignition and Flame Stabilization of a Premixed Jet in Hot Cross Flow, ASME Turbo Expo 2013: Turbine Technical Conference and Exposition, 2013.
[27] D.J. Micka, J.F. Driscoll, Stratified jet flames in a heated (1390 K) air cross-flow with autoignition, Combust. Flame 159 (2012) 1205-1214.
[28] J.A. Wagner, M.W. Renfro, B.M. Cetegen, Premixed jet flame behavior in a hot vitiated crossflow of lean combustion products, Combustion and Flame 176 (2017) 521-533.
[29] P.P. Panda, O. Busari, R.P. Lucht, W.R. Laster, Effect of the nature of vitiated crossflow on the flow-field of a transverse reacting jet, Experiments in Fluids 58 (2017) 9.
[30] P. Saini, I. Chterev, J. Pareja, M. Aigner, I. Boxx, Effects of Hydrogen-Enrichment on Flame-Holding of Natural Gas Jet Flames in Crossflow at Elevated Temperature and Pressure, Flow, Turbulence and Combustion 107 (2021) 219-243.
[31] M.J. Severin, O. Lammel, W. Meier, M. Aigner, Flame Stabilization Regimes of Lean Premixed Confined Jet Flames at Different Reynolds Numbers, 53rd AIAA/SAE/ASEE Joint Propulsion Conference2017.
[32] N. Docquier, S.b. Candel, Combustion control and sensors: a review, Prog. Energy Combust. Sci. 28 (2002) 107-150.
[33] J.G. Lee, D.A. Santavicca, Experimental Diagnostics for the Study of Combustion Instabilities in Lean Premixed Combustors, J. Propul. Power 19 (2003) 735-750.
[34] Y. Hardalupas, M. Orain, Local measurements of the time-dependent heat release rate and equivalence ratio using chemiluminescent emission from a flame, Combust. Flame 139 (2004) 188-207.
[35] C.M. Arndt, J.D. Gounder, W. Meier, M. Aigner, Auto-ignition and flame stabilization of pulsed methane jets in a hot vitiated coflow studied with high-speed laser and imaging techniques, Applied Physics B 108 (2012) 407-417.
[36] R. Sadanandan, M. Stöhr, W. Meier, Simultaneous OH-PLIF and PIV measurements in a gas turbine model combustor, Appl. Phys. B 90 (2008) 609-618.
[37] B. Renou, A. Boukhalfa, D. Puechberty, M. Trinité, Local scalar flame properties of freely propagating premixed turbulent flames at various Lewis numbers, Combust. Flame 123 (2000) 507-521.
[38] P. Trunk, I. Boxx, C. Heeger, W. Meier, B. Böhm, A. Dreizler, Premixed flame propagation in turbulent flow by means of stereoscopic PIV and dual-plane OH-PLIF at sustained kHz repetition rates, Proc. Combust. Inst 34 (2013) 3565-3572.
[39] S. Navarro-Martinez, A. Kronenburg, LES–CMC simulations of a lifted methane flame, Proc. Combust. Inst. 32 (2009) 1509-1516.
[40] M. Severin, Analyse der Flammenstabilisierung intensiv mischender Jetflammen für Gasturbinenbrennkammern, Ph.D. Dissertation, University of Stuttgart (2019).

[41] S.W. Grib, M.W. Renfro, Autoignition Stabilization of a Premixed Jet in Vitiated Coflow, 2018 AIAA Aerospace Sciences Meeting.